Dynamics and stability of an expanding laser-induced plasma in a low-density gas

V. Yu. Baranov, O. N. Derkach, V. G. Grishina, M. F. Kanevskii, and A. Yu. Sebrant
National Research Center-Kurchatov Institute, Moscow, 123098, Russia
(Received 16 March 1993)

Experimental studies of a laser-produced metal plasma expansion into a gas with a mass density of 0.1–30 $\mu g/cm^3$ have been performed using streak-camera imaging. The results show that plasma expansion dynamics can be described by a snowplow model with a dimension factor dependent on the laser focal spot shape. It has been shown that the plasma boundary becomes unstable at the moment of maximum deceleration (of the order of 10 $cm/\mu s^2$), and the evolution of boundary perturbation has been monitored. An explanation of the observed effect on the basis of Rayleigh-Taylor instability is proposed and confirmed by comparison of simple model predictions with experimental evidence. The evolution of the plasma-front profile has been observed for the times $0 < t < 10\gamma^{-1}$, where γ is the instability increment. Competition of different unstable modes has been observed.

PACS number(s): 52.25.−b, 52.35.−g

I. INTRODUCTION

Dynamics of a plasma plume in the ambient gas induced by a laser pulse at the incident intensities in the range 0.1–10 GW/cm^2 has been extensively studied for the past five years [1–7]. This plasma remains an interesting object for study for two reasons. On the one hand, three-dimensional dynamics of a compressive fluid is a very challenging scientific problem. On the other hand, laser-induced plasma processes are becoming important tools used for industrial processes of thin-film deposition [1,2]. There are several papers addressing the

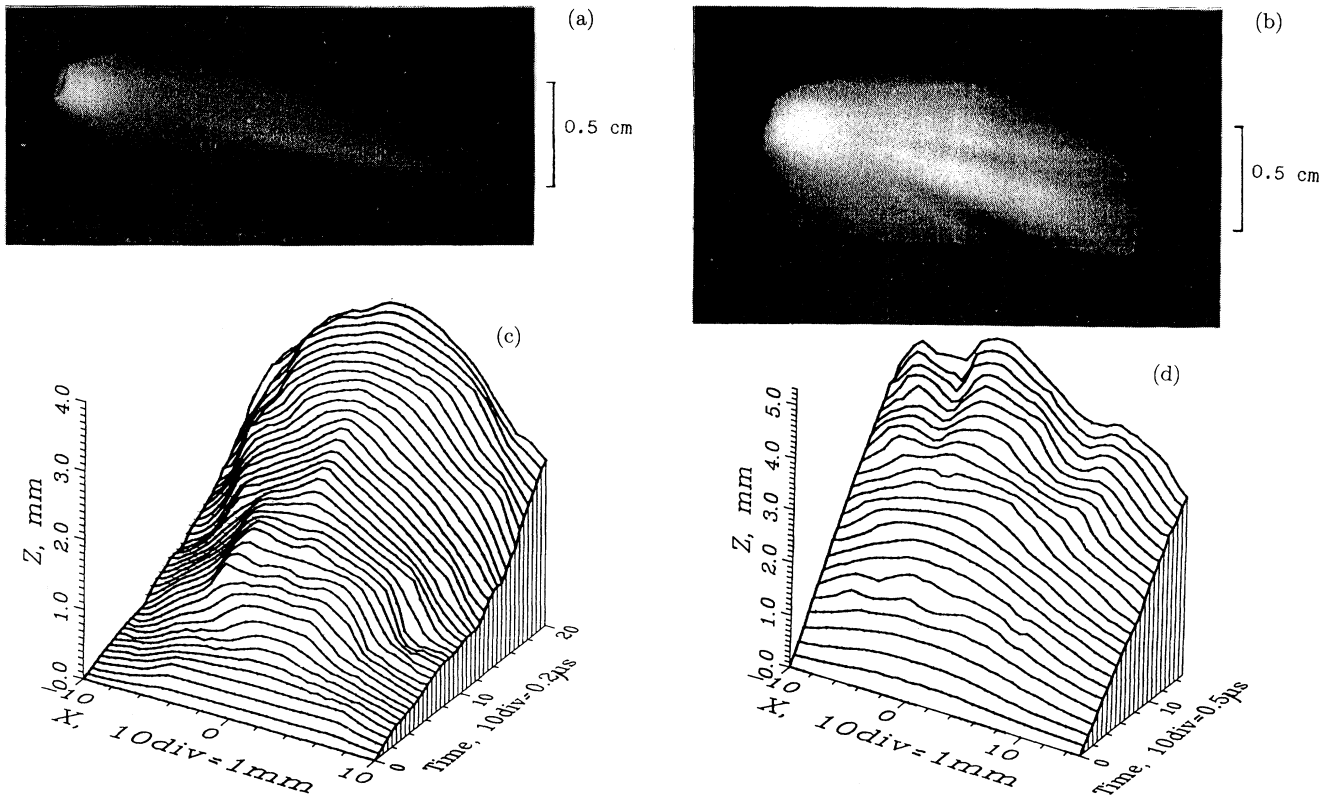

FIG. 1. (a) and (b) Integral photograph of Al plasma taken along the minor axis of elliptical focal spot. The XeCl short pulse (40 ns) horizontal laser beam is incident from the right while vapor plasma expands along the normal to the target surface. (c) and (d) Plots show space- and time-resolved plasma front profile evolution. Z, front coordinate along the direction of plasma propagation; X, distance along the minor axis of the focal spot. (a) and (c) air, $\rho_g = 0.5\ \mu g/cm^3$; (b) and (d) air, $\rho_g = 2.0\ \mu g/cm^3$.

stability of laser-induced plasma expansion in a low-density gas [3–7]. The results reported therein indicate that the plasma front often tends to become unstable and due to Rayleigh-Taylor instability the interface between the plasma and ambient gas becomes seriously perturbed.

In our earlier paper [3] we reported the observations of the evolution of spatial structures in a plasma induced by a short (40 ns) pulse of a XeCl laser operating at 308 nm. Even the simple integral photograph of the plasma at certain pressure in the chamber revealed evident jet-like structures (Fig. 1). Further studies were performed with streak cameras and monocromators so that both plasma-front trajectory and -front profile changes were recorded using the line emission of different plasma species. The results are also shown in Fig. 1. The laser spot on the target was elliptical with the axis ratio of approximately 3. Different target materials and gases (air, He, Kr) were used in the experiments. It was shown that (1) the plasma deceleration in the ambient gas can be reliably described by a "snowplow" model [8] assuming that the plasma-front velocity decreases because of the momentum transfer from the plasma to the gas; (2) plasma deceleration and the wavelength of plasma-front perturbation are controlled by the gas mass density, not pressure (similar results are observed when He pressure is 20 times that of Kr); (3) plasma expansion dynamics from the elliptical spot fits the model predictions for the expansion of a cylinder, and the observed plasma perturbations occur in layers parallel to the minor axis of the ellipse.

The results of these early experiments were interpreted as Rayleigh-Taylor instabilities. Later experiments performed with different lasers over a wide range of experimental conditions demonstrated that this effect can be observed in many cases. For example, some details of plasma emission spectra evolution in the case of plasma produced by 500-ns pulses of a XeCl laser at 20 GW/cm^2 could be explained by taking plasma-front instability into account [9].

It should be noted that, for long laser pulses ($\tau_p > 100$ ns), breakdown of the ambient gas often occurs and plasma plume structure becomes more complicated: it may consist of both target material plasma and gas plasma. This situation is also more complicated because for long pulses the model of instantaneous plasma formation and its further inertial expansion is no longer valid. Target evaporation and plasma production takes place over the length of time that is longer than the time typical of instability development.

To study target vapor plasma dynamics in the case when the plasma in the ambient gas can be easily induced at low pressure, we used a transversely excited atmospheric pressure (TEA) CO_2 laser with microsecond pulses. The wavelength of a CO_2 laser beam is 30 times longer than that of a XeCl laser and therefore plasma ignition thresholds are much lower [10].

II. EXPERIMENTAL TECHNIQUE AND FACILITIES

The Sverchok TEA CO_2 laser was used as a beam source in our experiments. This laser produces pulses at $\lambda = 10.6$ μm with energy 0.5 J, full pulse width 5 μs, and leading peak width 0.5 μs. A combination of lens and spherical mirror was used as a focusing system so that spot shape on the target can be varied from circular to elliptical with an axis ratio of 3 due to aberrations.

The diagnostic setup is shown in Fig. 2. Plasma image was projected onto the entrance slit of a streak camera. Two modes were used. When the plasma axis was parallel to the slit, plasma propagation dynamics was studied. When the plasma axis was normal to the slit and plasma regions at different distances from the target surface were projected onto the slit, plasma-front profile evolution was monitored. Spatial resolution in both modes was better than 0.1 mm in the object plane. Temporal resolution was 25 ns. The combination of two sets of experimental data made it possible to reconstruct the evolution of the plasma front profile as shown in Fig. 1. A more detailed description of this method is published elsewhere [11].

The target was placed in the vacuum chamber, which could be filled with different gases at a pressure in the range from 10^{-5} Torr to 1 atm. Several types of mechanical, thermocouple, and ionization vacuum gauges were used to measure the pressure. Laser-beam parameters were measured using an IKT-1 energy meter and a Ge:Au fast photodetector. Integral pictures of the plasma plume were taken by a camera with different color filters. At low pressure, a charge collector placed at a distance of 90 cm from the target was used for time-of-flight measurements. All electrical signals were recorded by an S9-8 digital storage oscilloscope and then processed with a personal computer connected to the oscilloscope through a standard IEEE 488 interface. The temporal resolution of this system was 50 ns. A He-Ne laser was used for preliminary adjustment of all the diagnostic equipment.

Targets were massive slabs of different metals (Cu, Mo, Al, W, and Pb) and graphite. They were mounted in the chamber on the translation and rotation stage controlled by stepping motors. Most of the experiments described in this paper were made with Pb targets.

Diagnostic equipment and techniques were similar to those used in the experiments [3,9]. This offered the op-

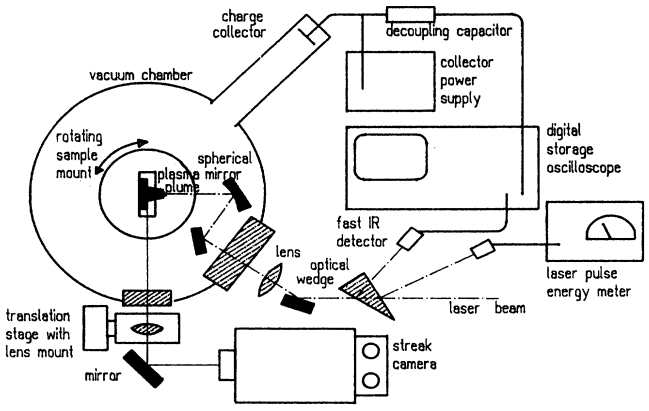

FIG. 2. The diagnostic setup used to study target vapor plasma dynamics in a low-pressure gas.

portunity to compare results obtained under similar conditions, but with different laser sources.

III. RESULTS AND DISCUSSION

A. Plasma front propagation and deceleration

Comparison of streak pictures and photos of the plasma for different axis ratios of the focal spot demonstrated that for a circular spot no distinct spatial structures are observed. This does not necessarily mean that the plasma expansion is stable; it may be that the perturbations are difficult to observe because of the integration of the picture along the line of sight. The most prominent structures are observed on both photographs and streak pictures when the focal spot axis ratio exceeds 3. Plasma-front trajectories at different pressures (and therefore gas mass densities) were compared with the predictions of a snow-plow model [8]. The momentum conservation equation in this model is

$$M_0 V_0 = [M_0 + \rho_g S_n (R^n - R_0^n)] \frac{dR}{dt} , \tag{1}$$

where $M_0 V_0$ is the initial momentum of the expanding plasma cloud with initial radius R_0, ρ_g is mass density of the ambient gas, S_n is the factor related to the area of the plasma-gas interface, R is the radius, and n denotes the system dimension. Depending on n, S_n can be expressed as follows: (i) for $n=1$, $S_1=S$, the spot area on the target for a flat one-dimensional (1D) expansion: (ii) for $n=2$, $S_2=L\pi/2\alpha$, where L is the spot larger axis and π/α is the angle of plasma expansion in the plane normal to larger spot axis; (iii) for $n=3$, $S_3=2\pi/\beta$, where $2\pi/\beta$ is the solid angle of the cone in which plasma expands.

For our experiments with a CO_2 laser, as in previous experiments with a short-pulse XeCl laser, $n=2$ proved to be the best fit for experimental data. For a focal spot with a different axis, pressure gradients acting along its major and minor axes are also different, and one may assume that no expansion occurs along the major axis. Anisotropy of the expansion in the direction of the minor axis was described by a factor α.

Figure 3 gives an example of the closeness of calculated and observed front trajectories for an air pressure of 3 Torr. The plots show that a 2D model can be used to calculate the plasma-front velocity and deceleration with sufficient precision.

Unlike the 1D model, the 2D approximation is characterized by an extremum in deceleration. Maximum deceleration is

$$\alpha_{\max} = \frac{25}{36} \frac{V_0^2}{3} \left[\frac{5}{9} \rho_g \frac{L\pi}{M_0 \alpha} \right]^{1/2} \tag{2}$$

and occurs at the moment when the front coordinate is

$$R(\alpha_{\max}) = \left[\frac{2M_0\alpha}{5\rho_g L\pi} \right]^{1/2} . \tag{3}$$

Then, using the dependence of $R(\alpha_{\max})^2 \rho_g$ on gas pressure (Fig. 4), one can determine how $M_0\alpha$ changes with pressure. It is evident from the plot that, with an increase of pressure, $M_0\alpha$ also slowly increases, i.e., that either the mass of evaporated material increases or the expansion occurs within a narrower angle. Additional experiments are required to tell which of the mechanisms is responsible for the observed effect. Note that an increase of the evaporated mass with pressure can be the result of the increase of the thermal coupling coefficient connected with plasma density and its emission of ultraviolet easily

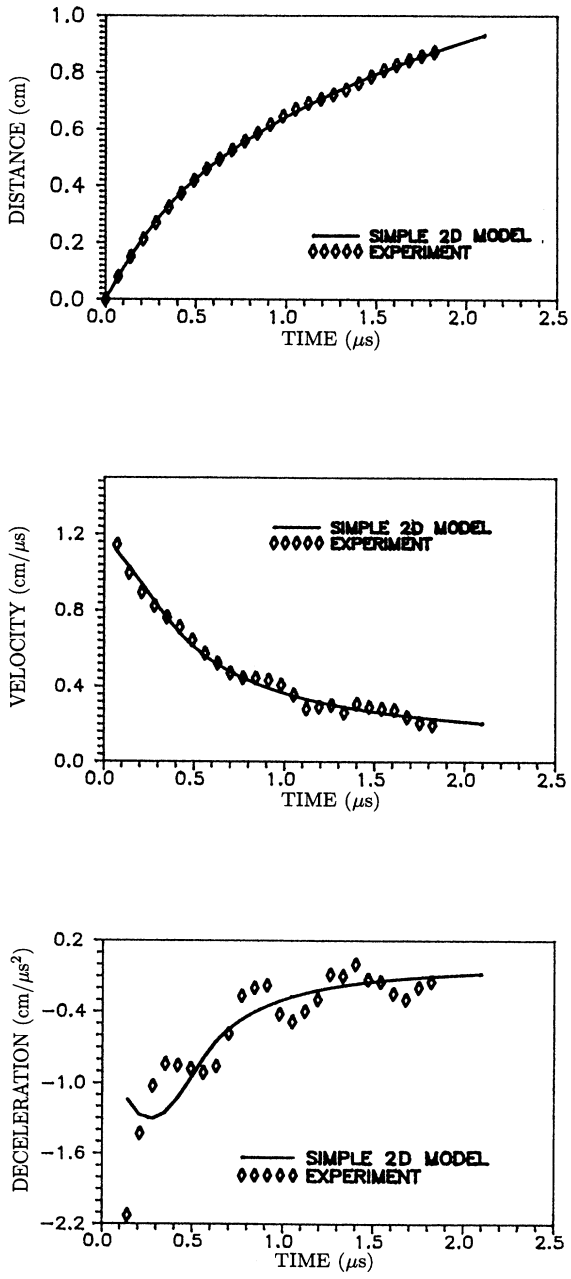

FIG. 3. Temporal evolution of the plasma-front coordinate, velocity, and deceleration: comparison of 2D model predictions and experimentally observed data. Air pressure $P=3$ Torr.

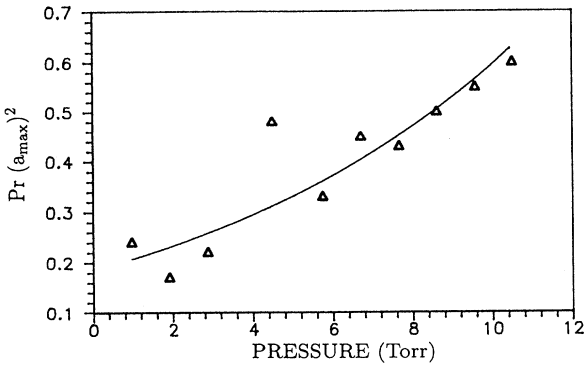

FIG. 4. The dependence of parameter $r(\alpha_{max})^2 P \propto M_0 \alpha$ on air pressure: both factors, mass growth and angle diminishing, can affect the parameter growth.

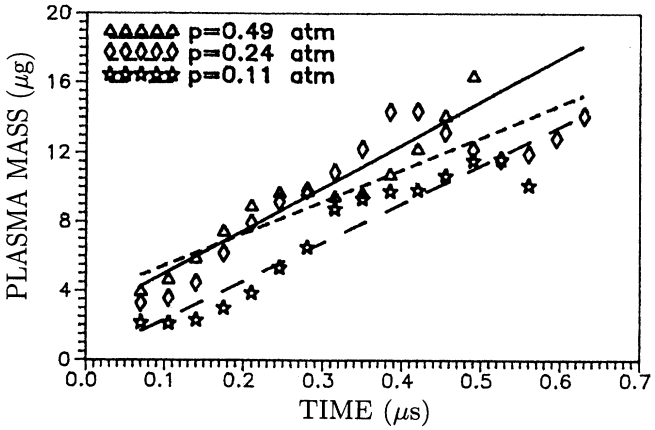

FIG. 5. Evaporated mass vs time for Al samples irradiated by XeCl laser at 30 GW/cm^2 with pulses of 500-ns duration. In a wide range of air pressure the rate of mass growth within the time of laser-pulse duration is almost constant.

absorbed by the target.

Estimations of α can be made on the basis of the measurements made with a charge collector. Rotating the target and changing the incident beam power to compensate for the changes of the spot size for different incidence angles, we could obtain the diagram of plasma expansion in vacuum. Integration of this dependence shows that if we assume uniform isotropic expansion, the parameter π/α should be approximately $\frac{1}{6}$ to give the observed total number of the particles. A decrease in the expansion angle with ambient gas pressure can be the result of decreasing its initial expansion velocity. Then the expansion tends to be closer to the 1D process when most of the particles move normal to the target surface.

A comparison of model computations with experimental plasma-front trajectories shows that in the pressure range where no optical breakdown occurs in the gas (0.1–10 Torr) the initial mass M_0 in Eq. (1) should be taken between 0.1 and 0.3 μg. Direct measurements of the cavity volume formed on a polished target shows that the mass removed by each laser pulse is 50 μg. Other studies of drilling with pulsed CO_2 lasers [10] show that in our experimental conditions about 30% of the total removed mass should be evaporated and the rest is removed as melt droplets. Since M_0 is only 0.2–0.6% of the total removed mass, one has to conclude that, in spite of the front deceleration, only a small fraction of the expanding plasma mass takes part in the momentum transfer to the gas while the rest of the plasma has no effect on plasma-front propagation.

Thus plasma-front dynamics in the case of 5-μs pulses of the CO_2 laser is essentially similar to that in the case of 40-ns XeCl laser pulses; in both cases the model of instantaneous explosion of a plasma with finite mass fits experimental results.

However, if a laser pulse is more intense and gas pressure is higher, a simple model with constant plasma mass is no longer valid. Curves plotted in Fig. 5 were obtained with XeCl laser pulses at 30 GW/cm^2 (pulse width, 500 ns). In this case, to fit the experimental data, one has to assume that M_0 increases linearly with time, $M_0 = \dot{m}(\rho)t$, for $0 < t < 350$–400 ns. After this phase of intensive evaporation, the plasma mass remains constant. In our experiments, $\dot{m} \approx 26$ g/s. Note that in these experiments the spot was circular and only the 3D version of Eq. (1) gave a good fit with the observed data. Results presented in Fig. 5 also demonstrate that $\dot{m}(\rho)$ is essentially constant over the pressure range between 0.1 and 1 atm. By the end of the pulse, the mass of the plasma that controls the front propagation is 9–11 μg, which is a noticeable fraction of the total removed mass (20–25 μg).

It should also be noted that at high pressures this simple technique based on measurements of plasma-front deceleration can be used for the estimation of the amount of evaporation material. This method is complementary to charge collectors and film-deposition techniques, which are good only for high vacuum experiments.

Later in this section we will demonstrate that in the presence of a laser-supported detonation wave in the beam of a CO_2 laser, plasma-front dynamics is more complicated and cannot be described using the simplest snow-plow model.

B. Plasma front stability

As we have shown above, the target material plasma expands in the ambient gas with deceleration. If the plasma mass density is higher than that of a gas, $\rho_t > \rho_g$, the gas-plasma interface becomes unstable due to well-known Rayleigh-Taylor instability.

Photographs of a plasma plume taken along the spot minor axis show distinct layers, similar to those obtained with XeCl laser pulses and shown in Fig. 1. This effect is also seen in the streak pictures taken with the camera slit normal to plasma axis. However, in this case we were using slower sweep rates than in experiment [3] and were able to observe more stages of instability development. Figure 6 presents several streak pictures of plasma taken at different distances from the target surface. Combining

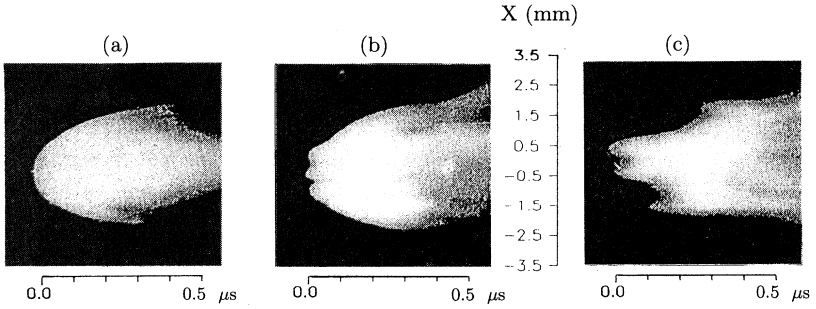

FIG. 6. Streak pictures of Pb vapor plasma taken at different distances Z from the target surface. Air pressure $P=3$ Torr. (a) $Z=0.2$ cm, (b) $Z=0.45$ cm, (c) $Z=0.75$ cm.

these pictures with a known plasma-front trajectory (for the axial part of the plasma), one can reconstruct the evolution of plasma profile versus time. The results are shown in Fig. 7.

Quasistationary development of Rayleigh-Taylor instability (at the stage of exponential growth) occurs when

$$\alpha k g t^2 > 1 , \tag{4}$$

where α and t are the plasma-front deceleration and the time of its action, respectively; $k=2\pi/r$ is the unstable mode wave vector (r is the observed period of plasma front growing (perturbation), $g=(\rho_t-\rho_g)/(\rho_t+\rho_g)$.

At the linear stage of instability development the perturbations with the shorter wavelengths exhibit the faster growth. As shown in [12–14], heat conductivity, viscosity, mass transfer across the plasma boundary, and a finite width of density drop are all stabilizing short-wave disturbances. When the amplitude of the perturbation becomes comparable to its period r, the rate of instability growth reaches its peak value, and after that moment long-wavelength instabilities grow faster. As a result, at the late stages of instability evolution, long period modes are dominant.

These considerations are confirmed by our experimental evidences. As noted in Ref. [3], at distances $z\approx 1-2$ mm from a target surface, where no significant distortion of a plasma front is observed, streak pictures show short-wavelength "ripples" on the front. Details of the ripples evolution are difficult to trace since they are not well repeated from shot to shot. However, at later stages well reproducible long-wavelength perturbations are observed (see Fig. 1).

An even more complicated evolution of plasma-front distortions is observed in our experiments with microsecond pulses of a CO_2 laser. As in previous work, we could not trace all the details of the evolution of initial small-scale perturbations. Distinct and reproducible perturbation of the plasma front is observed at $z>4.5$ mm. Typical spatial scale of these perturbations is close to $r=0.7$ mm. Using estimation (4), one can obtain a perturbation increment for a wave vector $k=2\pi r^{-1}$. As shown in Fig. 3, maximum deceleration occurs at the moment $t(\alpha_{\max})=0.28$ μs, and $\alpha_{\max}=1.5$ cm/μs^2. Under these conditions, the instability growth time is $t_{\text{ins}}=270$ ns. This is in good agreement with the experimentally observed value $t_{\text{ins}}=220$ ns. The modulation depth at this moment is 0.2 mm, which is comparable to r and therefore its growth is getting slower. Later, at $z=7$ mm, a structure with a larger spatial period, 1.5 mm, becomes dominant. However, when this new perturbation reaches the depth of 0.6 mm, the mode with $r=0.7$ mm becomes visible again. In other words, first the competition between the modes results in the development of the instability with the longest spatial period, but then at the nonlinear stage these begin to split into pairs again. This frequency doubling is often observed in nonlinear dynamic structures.

Now let us consider the effects leading to stabilization of the plasma boundary.

From Eq. (4) it is evident that the instability disappears when $g\to 0$, i.e., when $g_t\to g_g$. For constant laser-beam parameters, this happens when gas density is increased. In Refs. [3,11] we have demonstrated that both ways of increasing the gas mass density, increasing gas pressure or using a gas with heavier atoms, are equally efficient in suppressing the instability. Nonlinear dimensional analysis was used in this work to show that the number of observed layers N varies as $\rho_g^{1/3}/g$. This is in reasonable

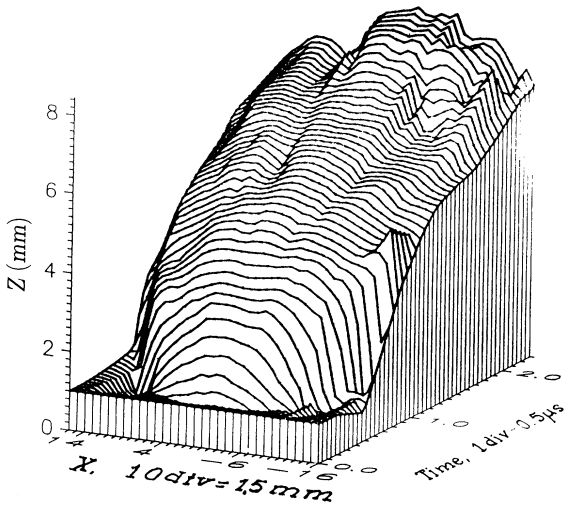

FIG. 7. Spatial and temporal evolution of Pb vapor plasma front expanding into air with pressure $P=3$ Torr. Reconstruction was made by combining streak pictures taken along the minor axis of the focal spot at different distances Z from the target surface (see Fig. 6) with axial streak picture (see Fig. 3, upper plot).

agreement with experimental observations. For $\rho_g > 50$ $\mu g/cm^3$ no perturbations were observed in the expanding plasma, and estimations show that g was close to zero at the distance where maximum deceleration of the plasma front occurs.

Another important and interesting way to suppress the instability is to ignite a laser-supported detonation (LSD) wave in a gas. Laser-beam absorption in the LSD wave changes the rate of target evaporation and gas density near the target plasma boundary. The effect is particularly clear in the case of CO_2 laser pulses, since LSD plasma shielding at $\lambda = 10$ μm is very strong. Streak camera pictures and plots of target plasma front propagation are shown in Fig. 8 for a XeCl laser with 500-ns pulses and in Fig. 9 for CO_2 laser pulses. For 10-μm pulses, the plasma front first accelerates and only later begins to decelerate, and this deceleration appears to be more gradual. The effect is illustrated by plots in Figs. 10 and 11, where the

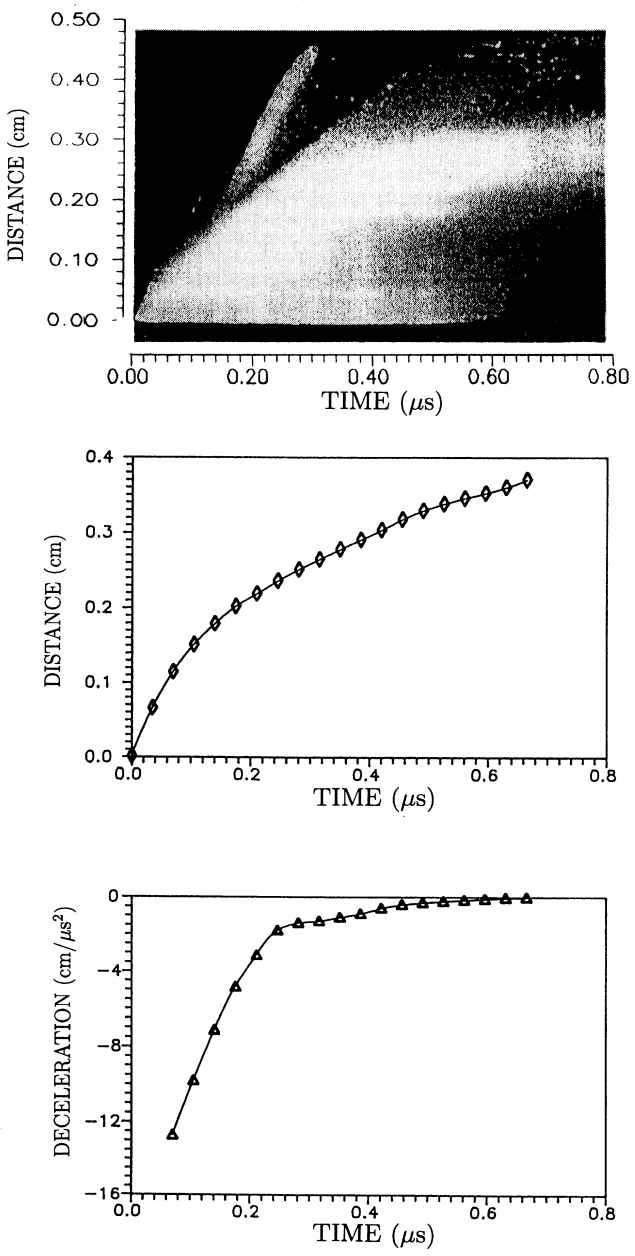

FIG. 8. Axial streak picture of Al vapor plasma expanding into air ($P = 86$ Torr) in the presence of the laser-supported detonation wave. Plots show vapor plasma front trajectory and front deceleration vs time. Both plasmas were ignited by XeCl laser-pulsed irradiation (pulse width, 500 ns).

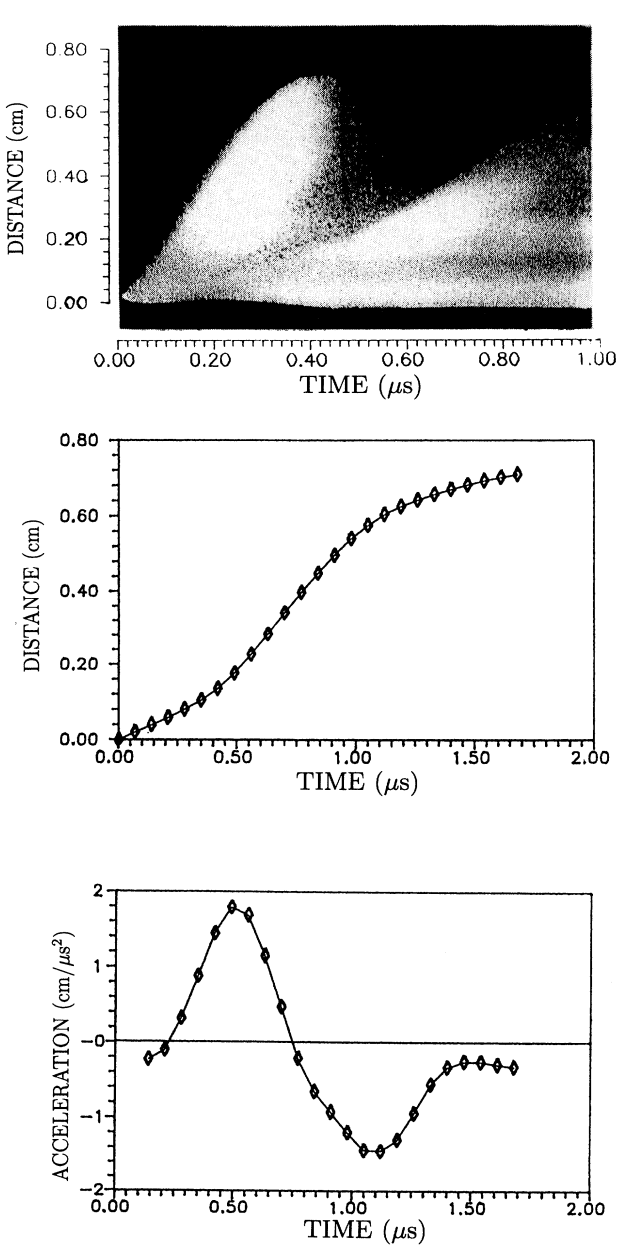

FIG. 9. Axial streak picture of Pb vapor plasma expanding into air ($P = 24$ Torr) in the presence of the laser-supported detonation wave. Plots show vapor plasma-front trajectory and -front deceleration vs time. Both plasmas were ignited by CO_2 laser-pulse irradiation (pulse width, 5 μs).

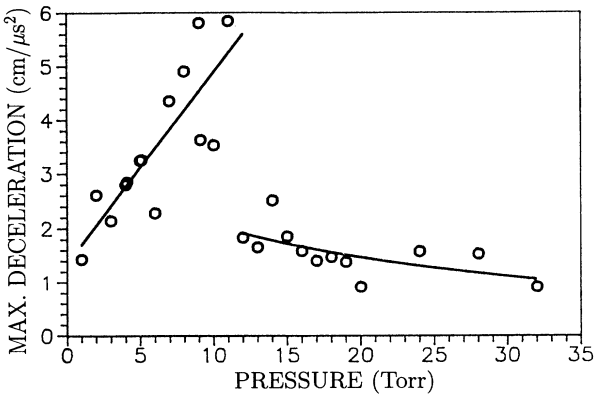

FIG. 10. Factors leading to the Rayleigh-Taylor instability suppression: magnitude of the maximum observed vapor plasma-front deceleration vs air pressure for the case of CO_2 laser-pulse irradiation.

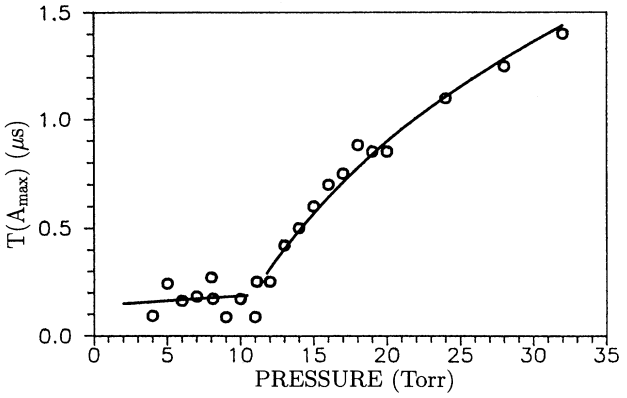

FIG. 11. Factors leading to the Rayleigh-Taylor instability suppression: time when the maximum of vapor plasma-front deceleration is observed vs air pressure for the case of CO_2 laser-pulse irradiation.

magnitude of the maximum observed front deceleration and the time when this maximum is observed are shown as functions of air pressure. Both curves demonstrate abrupt changes at the pressure equal to LSD ignition threshold.

IV. CONCLUSIONS

The main conclusions of this work are as follows.

(1) The prominent deformation of the front of the laser-induced plasma expanding in a low-pressure gas was observed for a wide range of experimental conditions.

(2) The explanation of the observed effect is proposed. The front perturbation is attributed to Rayleigh-Taylor instability of the decelerating plasma boundary. Estimations and experiments with gases of different mass density confirm this explanation.

(3) The stabilization of the front perturbations was observed and studied when a laser-supported detonation wave was ignited in the gas.

(4) Dynamics of an expanding plasma front was shown to be described by a simple snow-plow model with the dimension factor depending on the laser focal spot shape.

(5) The technique described in this paper seems to be very convenient for further studies of the instability. A number of experimental parameters can be varied easily: gas pressure, pulse width, amount of evaporated material, and its mass density. Controlled regular perturbations can be introduced easily at the initial stages of plasma expansion if grids with different mesh size are used instead of solid flat targets.

ACKNOWLEDGMENTS

The authors would like to express their gratitude to D. D. Malyuta and M. A. Stepanova for their constant interest in the work, and to V. N. Anisimov and Yu. V. Vlazneva for their assistance in the experiments and data processing. This work was supported in part by the United States Department of Defense.

[1] *Laser and Particle-Beam Chemical Processing for Microelectronics,* edited by Daniel J. Ehrlich, Gregg S. Higahi, and Modest M. Oprysko (Materials Research Society, Pittsburgh, 1988), p. 500.

[2] A. D. Ahsahalyan *et al.,* J. Tech. Phys. **52**, 1584 (1982); **52**, 1590 (1982); **52**, 1843 (1982).

[3] L. A. Bolshov *et al.,* Dynamics of expansion of metal plasma produced by pulses of XeCl laser. Izv. Akad. Nauk SSSR, Ser. Fiz. **52**, 1852 (1988).

[4] S. V. Gusev *et al.,* in *Papers Abstracts of VII All-Union Conference on Interaction of Optical Beams with Matter, Leningrad, 1988* (GOI, Leningrad, 1988), pp. 164 and 165.

[5] A. N. Panchenko and V. F. Tarasenko, Fiz. Plasmy **14**, 761 (1988) [Sov. J. Plasma Fiz. **14**, 450 (1988)].

[6] O. B. Anan'in *et al.,* Kvant. Electr. (Moscow) **14**, 2313 (1987) [Sov. J. Quantum Electron. **17**, 1474 (1987)].

[7] O. B. Anan'in *et al.,* Fiz. Plasmy **17**, 877 (1991) [Sov. J. Plasma Phys. **17**, 513 (1991).

[8] D. W. Koopman, H.-L. Siebeneck, and G. Jellison, Phys. **17**, 513 (1991); Phys. Fluids **22**, 526 (1979).

[9] V. N. Anisimov *et al.,* Laser Phys. **1**, 188 (1991).

[10] R. V. Arutynuyan *et al., Laser Beam Effects on Materials* (Nauka, Moscow, 1989), p. 368.

[11] M. F. Kanevskii, A. Yu. Sebrant, and S. Yu. Chernov, *Dynamics of Near-Surface, Low-Temperature, Laser-Induced Plasmas* (IAE, Moscow, 1990), p. 144.

[12] D. L. Youngs, Physica D **12**, 32 (1984).

[13] R. G. Evans, Can. J. Phys. **64**, 893 (1986).

[14] E. G. Gamalii *et al.,* Tr. Fiz. Inst. Akad. Nauk SSSR **134**, 73 (1982).

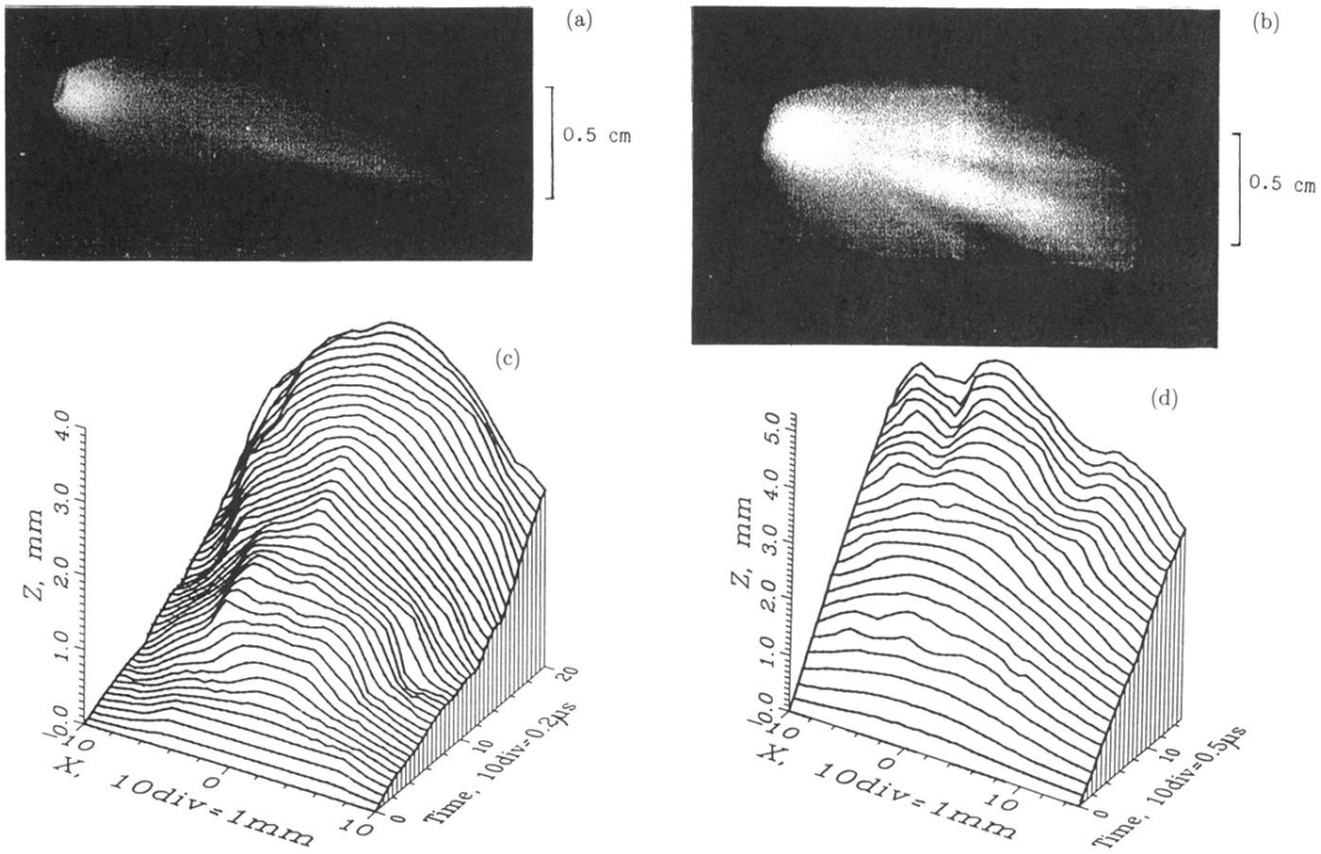

FIG. 1. (a) and (b) Integral photograph of Al plasma taken along the minor axis of elliptical focal spot. The XeCl short pulse (40 ns) horizontal laser beam is incident from the right while vapor plasma expands along the normal to the target surface. (c) and (d) Plots show space- and time-resolved plasma front profile evolution. Z, front coordinate along the direction of plasma propagation; X, distance along the minor axis of the focal spot. (a) and (c) air, $\rho_g = 0.5\ \mu g/cm^3$; (b) and (d) air, $\rho_g = 2.0\ \mu g/cm^3$.

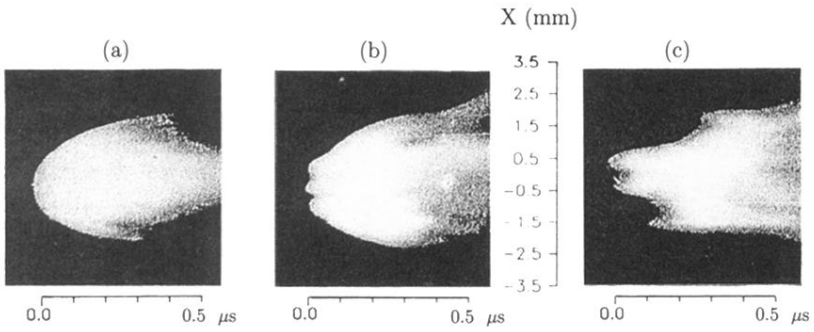

FIG. 6. Streak pictures of Pb vapor plasma taken at different distances Z from the target surface. Air pressure $P=3$ Torr. (a) $Z=0.2$ cm, (b) $Z=0.45$ cm, (c) $Z=0.75$ cm.

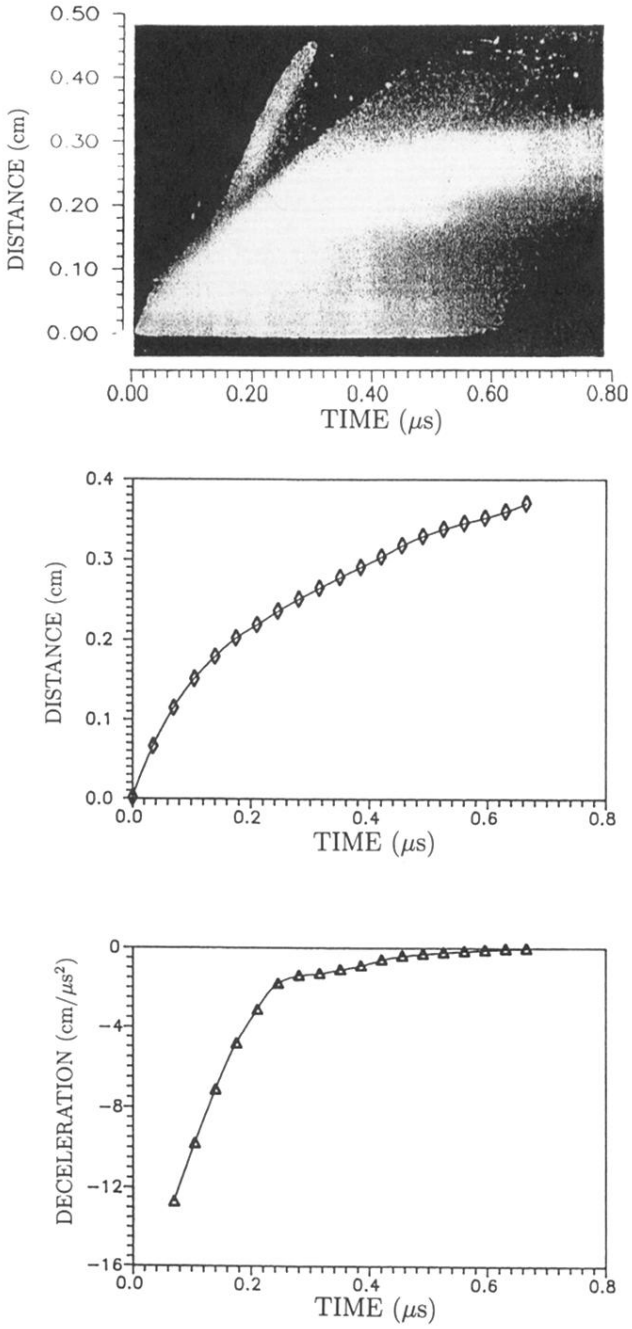

FIG. 8. Axial streak picture of Al vapor plasma expanding into air ($P = 86$ Torr) in the presence of the laser-supported detonation wave. Plots show vapor plasma front trajectory and front deceleration vs time. Both plasmas were ignited by XeCl laser-pulsed irradiation (pulse width, 500 ns).

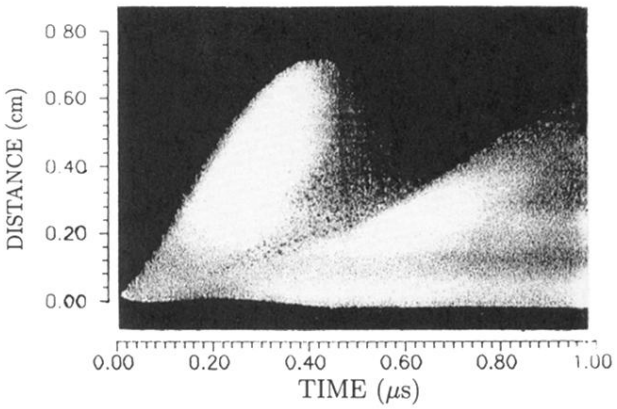

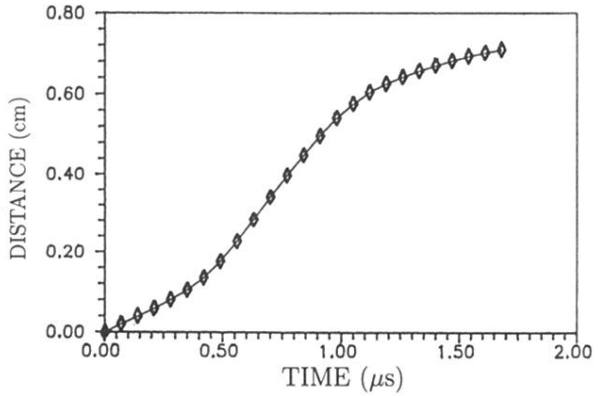

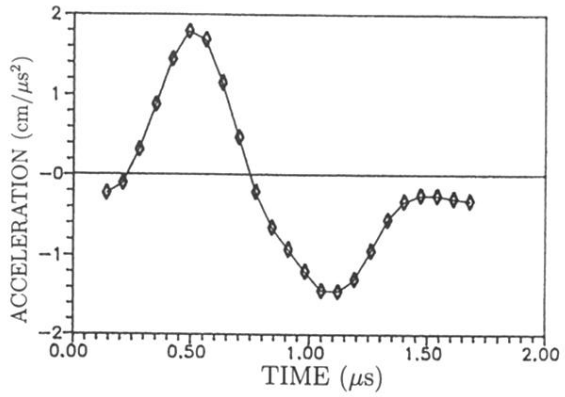

FIG. 9. Axial streak picture of Pb vapor plasma expanding into air ($P = 24$ Torr) in the presence of the laser-supported detonation wave. Plots show vapor plasma-front trajectory and -front deceleration vs time. Both plasmas were ignited by CO_2 laser-pulse irradiation (pulse width, 5 μs).